An experimental study into the effect of injector pressure loss on self-sustained combustion instabilities in a swirled spray burner

Guillaume Vignat, Daniel Durox, Kevin Prieur, Sébastien Candel

An Experimental Study into the Effect of Injector Pressure Loss on Self-Sustained Combustion Instabilities in a Swirled Spray Burner

Guillaume Vignat[a,*], Daniel Durox[a], Kevin Prieur[a,b], Sébastien Candel[a]

[a] *Laboratoire EM2C, CNRS, CentraleSupélec, Université Paris-Saclay, 3, rue Joliot Curie, 91192 Gif-sur-Yvette, France*
[b] *Safran Tech, E&P, Châteaufort, CS 80112, 78772, Magny-Les-Hameaux, France*

Abstract

Combustion instabilities depend on a variety of parameters and operating conditions. It is known, especially in the field of liquid rocket propulsion, that the pressure loss of an injector has an effect on its dynamics and on the coupling between the combustion chamber and the fuel manifold. However, its influence is not well documented in the technical literature dealing with gas turbine combustion dynamics. Effects of changes in this key design parameter are investigated in the present article by testing different swirlers at constant thermal power on a broad range of injection velocities in a well controlled laboratory scale single injector swirled combustor using liquid fuel. The objective is to study the impact of injection pressure losses on the occurrence and level of combustion instabilities by making use of a set of injectors having nearly the same outlet velocity profiles, the same swirl number and that establish flames that are essentially identical in shape. It is found that combustion oscillations appear on a wider range of operating conditions for injectors with the highest pressure loss, but that the pressure fluctuations caused by thermoacoustic oscillations are greatest when the injector head loss is low. Four types of instabilities coupled by two modes may be distinguished: the first group features a lower frequency, arises when the injector pressure loss is low and corresponds to a weakly coupled chamber-plenum mode. The second group appears in the form of a constant amplitude limit cycle, or as bursts at a slightly higher frequency and is coupled by a chamber mode. Spontaneous switching between these two types of instabilities is also observed in a narrow domain.

Keywords:
Combustion Instabilities, Swirled flames, Spray flames, Injection Dynamics, Pressure Loss

*Corresponding author:
Email address: guillaume.vignat@centralesupelec.fr
(Guillaume Vignat)

1. Introduction

Combustion instabilities induced by an acoustic coupling are a recurring problem in high performance devices like aero-engines, liquid rocket motors and gas turbines for energy production. A substantial research effort has been dedicated to the understanding of the driving mechanisms and to the development of models, predictive tools and design control methods that could be used to avoid or suppress these dynamical phenomena. Much of the early work was motivated by spectacular failures of liquid rockets [1–4]. Research in the recent period has focused on issues related to gas turbines operating in the premixed mode (see for example the reviews [5, 6]). The effort in control has mainly been aimed at increasing the acoustic damping rate in the chamber using quarter wave tubes, Helmholtz resonators, acoustic liners, bias flow perforated plates, etc. [4, 7–12]. An alternative route has been used that consisted in changing the acoustic mode structure and resonance characteristics of the system by placing baffles in the chamber. This method has been widely used in rocket engines to remove transverse oscillations (see for example [13]). A segmentation of the annular plenum of the combustor has also been used to reduce instabilities coupled by azimuthal modes in an industrially produced gas turbine [14]. Other studies have explored the possibility of changing the flame pattern and flame dynamics to reduce their sensitivity to perturbations and diminish the gain of the process that drives the instability, leading to the suppression of the unstable acoustic-combustion coupling [12, 15–17]. A significant research effort has also been made to develop active control methods for combustion instability reduction [18, 19], with successful laboratory scale demonstrations and industrial application in some gas turbines [12] but these methods have generally been considered to be too complex for a generalized implementation.

One method that has been extensively exploited in rocket engines has consisted in implementing a pressure drop in the injection elements to decouple the upstream manifold dynamics from those of the thrust chamber [1–3]. Relative injector pressure drop values of the order of 10 to 15% are typically adopted in engineering practice. Such head losses cannot be used in gas turbines, because of their impact on the overall engine thermodynamic efficiency. It is however important to examine effects of injector pressure losses on combustion instability and see how this parameter influences the stability of the system, an issue that has not been extensively investigated. In gas turbine combustors, the injection pressure of the liquid fuel is much higher than the chamber

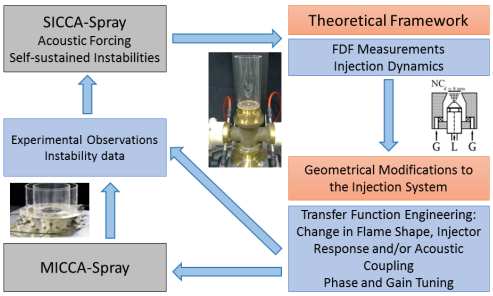

Figure 1: Test methodology combining experiments on a single injector system and on the annular model scale combustor MICCA-Spray. The objective is to guide experimentation by tailoring the dynamical response.

pressure to promote atomization and one may assume that the fuel manifold is insensitive to pressure perturbations in the chamber. However, pressure losses in the air stream have relatively low values of the order of a few percent (typically 3 to 4%). When modifying the head loss level in a swirled premixed burner by varying the pressure drop across the swirling injector Polifke et al. [20] observed that for certain operating conditions, an increase in air flow rate in the injector led to the triggering of an instability. They also noted that this corresponded to a change in the slope of the operating line linking the air flow rate to the pressure drop and attributed this effect to a change in the recirculation zone at the injector outlet and thus to a change of flame geometry that in turn led to a change in the flame response to perturbation promoting instability.

The question that can be raised is whether an increase in the pressure drop of the air stream across injectors, without any significant change in flame shape and dynamics, can change the stability characteristics of the system possibly reducing or suppressing instabilities. This question is investigated in the present article. It is of course linked to the possible acoustic coupling between the upstream plenum and the combustion chamber. It is known that these cavities are weakly coupled if there are large changes in cross sections [21–23]. The coupling may also be changed by the injector pressure drop that modifies the injector impedance. It is then worth considering injectors with different head losses but similar swirl numbers conserving the flame shape and examining the flame dynamics and corresponding self-sustained oscillations. A single injector configuration is used in the present investigation (designated as “SICCA-Spray”) but the analysis is carried out in a framework where tests on this geometry are used to prepare investigations on a more complex multiple injector annular configuration “MICCA-Spray” at EM2C

laboratory. Strong azimuthally coupled combustion instabilities have already been observed in MICCA-Spray [24] and it was shown that injectors operating near the pressure antinodes were essentially driven by velocity perturbations induced by the injector response to the azimuthal mode. It is then logical to use the iteration loop shown in Fig. 1 to characterize the dynamics of injectors, measure flame describing functions (FDF) using acoustic forcing or examine the dynamics of the system under self-sustained, longitudinally coupled, combustion oscillations. The FDF can then be included in the stability analysis as exemplified in [25] in a configuration featuring longitudinal acoustic modes or implemented in combination with a Helmholtz solver as explored in [26]. The pressure loss across the injector is here considered as a design parameter that can be varied to promote or reduce unstable oscillations. Results obtained in single element tests can be used to guide experimentation on the MICCA-Spray annular system.

This article describes experiments carried out only on the single injector spray swirled burner SICCA-Spray. This configuration is briefly described in Sec. 2. Four different injectors are designed (Sec. 3) with the same swirl numbers, in order to have identical flame shapes, but different pressure drops (up to 30% difference). A stability map of this system is constructed in Sec. 4 by keeping the thermal power constant and exploring a broad range of injection velocities. Results are interpreted in Sec. 5.

2. Experimental Setup

The SICCA-Spray experiment [27] is sketched in Fig. 2. This single injector version of the MICCA-Spray annular combustion chamber [24] comprises a combustion chamber, a plenum, fed with compressed air, and an injector fed with air from the plenum and with liquid n-heptane fuel. The chamber is formed by a quartz tube of length $l_c = 315\,\text{mm}$. The base of the chamber has a 15 mm high section made of brass. The injection system comprises a main body (grey), an interchangeable swirler and an atomizer for the liquid fuel. The atomizer produces a hollow cone shaped spray of liquid fuel droplets. Their Sauter mean diameter measured 2.5 mm above the injector outlet is $d_{32} = 35\,\mu\text{m}$ [27]. The injector ends in a conical convergent section, with an exit radius of $R_{inj} = 4\,\text{mm}$. The swirler is manufactured using a stereolithography 3D printer. It consists in a hollow cylinder with six tangential cylindrical channels. Key dimensions and notations are shown in Fig. 3. Two Monacor SP-6/108 Pro driver units are mounted on the plenum. They are not used in this study, and their

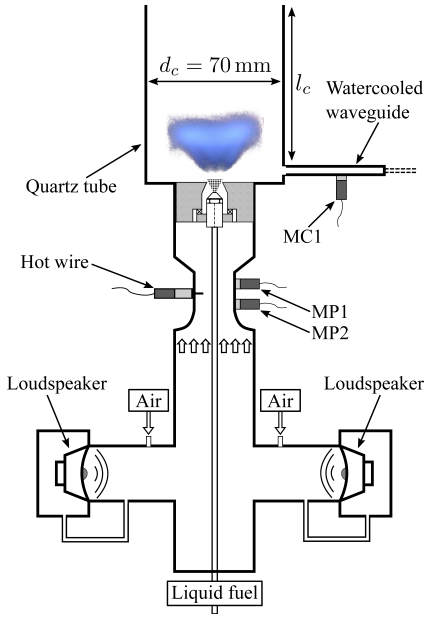

Figure 2: Schematic representation of the SICCA-Spray setup.

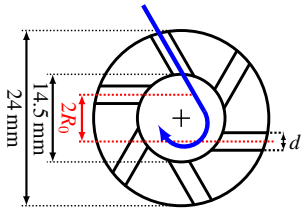

Figure 3: Schematic view of the swirler seen from above indicating the main dimensions of this component. d is the diameter of the small cylindrical tangential channels, and R_0 is the distance between the axis of the channels and the swirler centerline.

electrical circuit is left open. A straight tubular section upstream of the injector is used for measurements in the plenum. The fuel mass flow rate is measured using a Bronkhorst mini CORI-FLOW mass flow meter of relative accuracy ±0.4 %, and similarly, the air mass flow rate is measured using a Bronkhorst El-Flow thermal mass flow meter of relative accuracy ±0.9 %. In this article, the bulk velocity $u_b = \dot{m}/(\pi\rho R_{inj}^2)$ is defined as the 1D velocity at the injector outlet under cold flow conditions.

Head loss is measured using a Kimo MP111 differential pressure gauge, with a 1% relative precision. Three Bruel & Kjaer type 4938 microphones with type 2670 preamplifier detect acoustic pressure signals. Their relative accuracy is 1% and their cut-off frequency of 70 kHz is far greater than the sampling frequency of 16 384 Hz used for data acquisition. Microphone MC1 is used to measure the pres-

Table 1: Dimensions and characteristics of the swirlers considered in this study.

	d (mm)	R_0 (mm)	S	σ
S_a	2.9 ± 0.1	2.3 ± 0.1	0.65	4.3
S_b	3.3 ± 0.1	3.0 ± 0.1	0.64	4.1
S_c	3.6 ± 0.1	3.5 ± 0.1	0.64	3.7
S_d	4.0 ± 0.1	4.6 ± 0.1	0.60	3.6

sure at the backplane. It is mounted on a water-cooled wave guide. This microphone is at 290 mm from the chamber backplane. Microphones MP1 and MP2 are mounted flush to the wall of a straight tubular section of the plenum upstream of the injector. They are separated by 50 mm. Combined with a Dantec Dynamics miniCTA constant temperature hot wire anemometer (cutoff frequency 10 kHz), they are used to measure acoustic pressure and velocity upstream of the injector. A Dantec Dynamics FlowExplorer two component Laser Doppler anemometer (LDA) measures velocities 2.5 mm downstream the combustor backplane, under non-reactive conditions and without the quartz tube. The theoretical optical probe volume of this LDA system measures 0.14 mm × 0.14 mm × 0.23 mm. Measurements are spaced every 0.25 mm. Uncertainty on the measured mean velocities, taking statistical uncertainties into account, is less than 0.8 m s^{-1}. Finally, a Princeton Instruments PiMax4 camera is used for flame visualization. An optical bandpass filter centered on $\lambda = 430$ nm is used to restrain visualization to light emitted by CH*.

3. Design of the injectors

Four injection systems were designed by changing the swirler units, while trying to keep the same flame shape and outlet velocity profiles as the reference injector used in [24]. To do so, a large parameter sweep was performed on parameters d and R_0 of the swirlers (see Fig. 3). A total of 38 swirlers were manufactured, the velocity profile at their outlet were measured using the LDA system and the flame shape was determined using CH* chemiluminescence. Their experimental swirl number S is calculated using the conventional expression

$$S = \frac{\int_0^{2R_{inj}} \overline{U_\theta}\,\overline{U_x}\, r^2 dr}{R_{inj} \int_0^{2R_{inj}} \overline{U_x}^2 r dr} \quad (1)$$

Among the 38 swirlers, four were selected and named S_a to S_d. Table 1 gathers key geometrical characteristics and aerodynamic performances. These four swirlers have very similar swirl numbers, and a nearly identical outlet mean velocity profile, shown in Fig. 4. The RMS velocity profiles (not presented here) show only a very small difference between the different swirlers. The injector head loss ΔP is shown in Fig. 5 for each swirler. Its evolution with the bulk velocity follows the usual scaling law: $\Delta P = 1/2\,\rho\sigma u_b^2$. The value of σ for each swirler is indicated in Tab. 1.

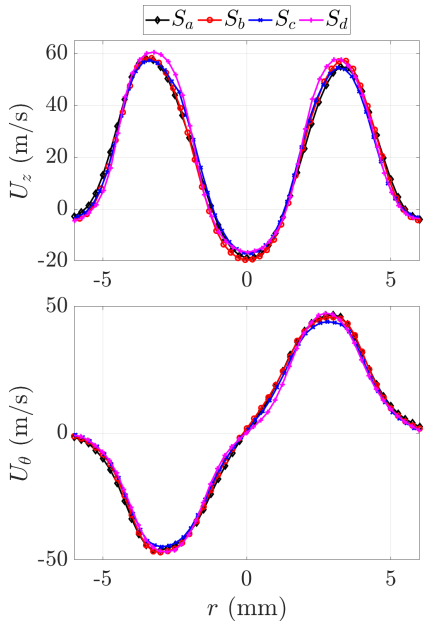

Figure 4: Mean axial (U_z, top) and azimuthal (U_θ, bottom) velocity profiles measured 2.5 mm downstream of the injector under cold flow conditions outlet using LDA. $u_b = 43$ m s^{-1}.

Figure 6 shows a direct visualization of CH* chemiluminescence from the four flames at ($\mathcal{P} = 6.2$ kW, $\phi =$

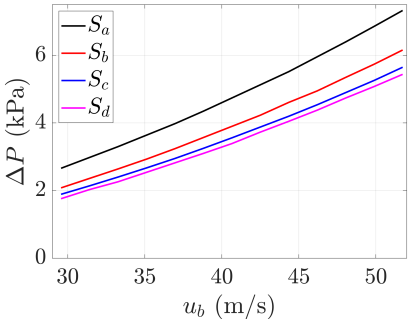

Figure 5: Head loss ΔP of each swirler for the range of bulk air velocity used in this study. It is the difference between the pressure in the plenum, measured at position MP2, and the ambient pressure, in the absence of combustion.

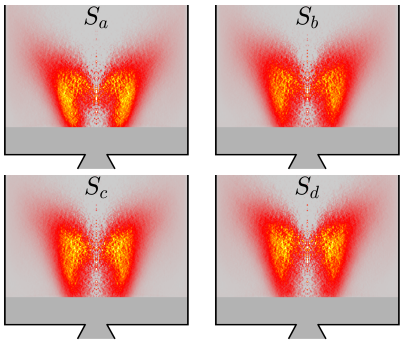

Figure 6: CH* chemiluminescence image of the stable flame obtained by reducing the combustion chamber length to 165 mm. The line-of-sight integrated images obtained by the PiMax4 camera are Abel transformed. Yellow and white correspond to high light intensities while gray corresponds to no light. No information is available near the backplane due to the opaque brass section at the bottom of the combustion chamber. Positions of the quartz confinement tube and conical injector outlet are also indicated. Swirler S_a to S_d. Operating condition: ($\mathcal{P} = 6.2\,\mathrm{kW}, \phi = 0.98, u_b = 36\,\mathrm{m\,s^{-1}}$).

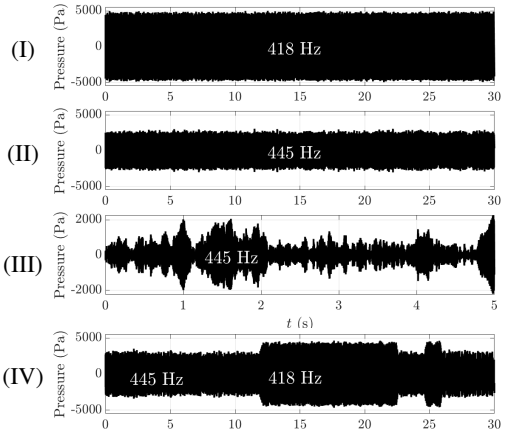

Figure 7: Typical pressure records p_c measured by microphone MC1 at the combustor backplane illustrating type (I) to (IV) instabilities, as indicated on the left of each graph. The power is kept constant $\mathcal{P} = 6.2\,\mathrm{kW}$. Type (I) instability is mainly observed with swirlers S_b, S_c and S_d; type (II) instability is observed with the four swirlers; type (III) instability is observed with the four swirlers near the borders of the unstable domain; type (IV) instability is only observed with swirler S_c.

0.98, $u_b = 36\,\mathrm{m\,s^{-1}}$). These four images are obtained by averaging over 900 frames with 0.1 ms exposure time each. It shows that the four flames have similar "M"-shapes and this has been verified for wide range of operating points.

4. Different types of combustion dynamics

The presence of self-sustained combustion instabilities in the SICCA-Spray experiment is investigated for each of these injection systems. The thermal power is kept constant at $\mathcal{P} = 6.2\,\mathrm{kW}$, while the air mass flow rate is varied, so that u_b varies between 29 and $51\,\mathrm{m\,s^{-1}}$, corresponding to global equivalence ratios between $\phi = 1.18$ and 0.69. The acoustic pressure near the combustor backplane p_c is measured by microphone MC1.

Five distinct types of dynamical regimes may be distinguished depending on the injection system and operating point:

(I) Limit cycle at approximately 418 Hz;
(II) Limit cycle at approximately 445 Hz;
(III) Bursts;
(IV) Spontaneous and irregular switching between type I and II instabilities;
(V) No oscillations or low amplitude perturbations : the peak acoustic pressure level in the chamber is less than 300 Pa.

Typical examples of pressure signals recorded near the combustor backplane are shown in Fig. 7 to illustrate these behaviors. The frequency of the burst regime is closest to 445 Hz, but it does vary on a wide range depending on the operating conditions, reaching as low as 425 Hz.

Figure 8 shows the type of instability that was observed for each swirler in SICCA-Spray when varying the air mass flow rate while keeping the power constant at $\mathcal{P} = 6.2\,\mathrm{kW}$. Great care was taken to wait for the experiment to reach thermal equilibrium in order to eliminate the thermal environment impact on stability, an effect that is well known (see for example [24]). No hysteresis phenomena were observed.

Swirler S_a with the highest head loss is unstable over a wider range of operating conditions. Only type (II) and (III) instabilities at $f = 445\,\mathrm{Hz}$ are observed with this swirler. The burst regime appears for both the leanest and the richest operating points. As the head loss decreases with swirlers S_b, S_c and S_d, the range of unstable operating conditions narrows. For swirler S_b, the first oscillations are in the burst regime, before switching to a limit cycle at 418 Hz near the stoichiometry. However, the instability rapidly switches to 445 Hz as the air flow rate is increased. For swirler S_c, the first unstable point appears at stoichiometric conditions, and a limit cycle at 418 Hz is observed. This type (I) instability arises over a broad range of operating conditions. Switching between 418 Hz and 445 Hz limit cycles takes place for $\phi = 0.83$. For leaner operating conditions, as for the other swirlers, a 445 Hz limit cycle is established giving rise to bursts at lower air flow rates.

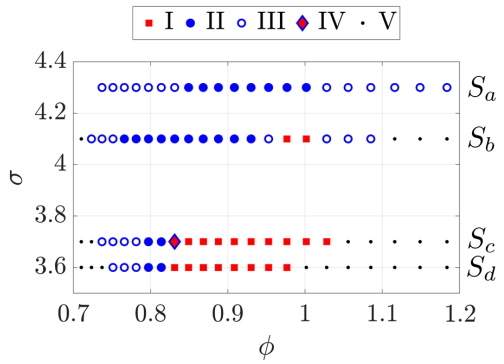

Figure 8: Instability map showing the different types of combustion instabilities observed as a function of equivalence ratio ϕ and head loss coefficient σ of the swirlers. Red square: Limit cycle at 418 Hz, Open blue circle: Limit cycle at 445 Hz, Solid blue circle: Bursts, Red diamond: Switching between type I and type II, Dot: No oscillation.

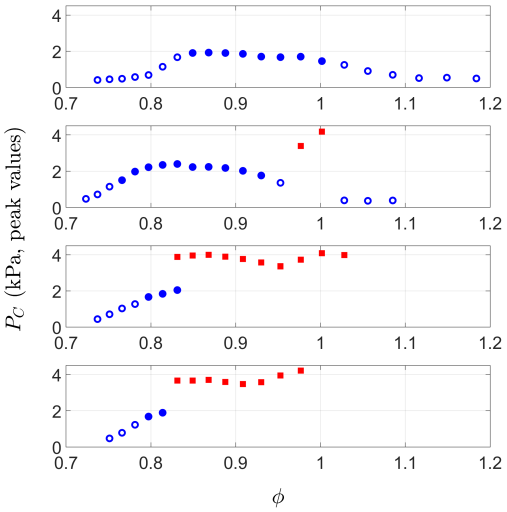

Figure 9: Acoustic pressure amplitudes measured at the combustor backplane during thermoacoustic oscillations. Symbols are identical to those used in Fig. 8.

Swirler S_d, compared to swirler S_c, behaves similarly, but has a slightly narrower range of unstable conditions.

Figure 9 shows the amplitude of the acoustic pressure near the combustor backplane for the operating points appearing in Fig. 8. The level is always higher when the thermoacoustic oscillation frequency is around 418 Hz (red squares on Fig. 9). It reaches a peak level between 3400 and 4200 Pa while it is always inferior to 2400 Pa when the frequency is around 445 Hz (blue circles in Fig. 9).

5. Discussion

The coexistence of two types of combustion instabilities in a system can often be attributed to the coexistence of two flames having a different shapes and dynamical responses [20, 28, 29]. To investigate this point, phase-averaged CH* chemiluminescence imaging of swirler S_c at operating condition ($\mathcal{P} = 6.2\,\mathrm{kW}, \phi = 0.83, u_b = 42\,\mathrm{m\,s^{-1}}$) was used. At this operating point, type (IV) instabilities with alternating limit cycles were observed (see Fig. 7).

In Fig. 10, the phase averaging is conditioned with respect to the thermoacoustic oscillation signal. This allows a direct comparison of flame shapes between the two combustion instabilities at a single operating point. The flames appear identical in the two types of oscillations, indicating that the coexistence of the two instabilities is not caused by a change in flame shape.

It is then natural to inquire if this may be linked to the acoustic eigenmodes of the system by making use of the Helmholtz solver of COMSOL Multiphysics. The geometry includes an end correction for the quartz confinement tube $\Delta l = 0.4 \times d_c$ where d_c is the diameter of the tube (see Fig. 2). At that distance from the chamber exit, the acoustic pressure vanishes. The passive loudspeakers in the plenum are not well characterized acoustically. In order to evaluate the influence of the plenum on the acoustic structure of the system, the acoustic impedance of the whole plenum was experimentally measured by making use of the three microphone method described by Chung and Blaser [30]. A third microphone replaces the hot wire in this experiment, and the combustion chamber and injector are replaced by a loudspeaker mounted at the end of a tube used to generate plane waves in the system. The impedance is reconstructed in a plane defined by the hot wire position in Fig. 2. The plenum can then be replaced by an impedance boundary condition in the simulations. All other boundary conditions correspond to rigid walls. The speed of sound and fluid density are assumed to be uniform in the chamber and the plenum respectively.

Acoustic response simulations are compared with experimental data in Tab. 2 for swirler S_d. In these experiments, a loudspeaker placed next to the SICCA-Spray setup provides acoustic excitation. In a first case, in the left column of Tab. 2, the experiment is carried out with air at room temperature in the absence of flow. In the second (third column of Tab. 2), the combustion chamber is filled with a mixture of helium and air in a suitable proportion that yields a speed of sound coinciding with that prevailing under hot fire conditions. Experimental data (columns 1 and 3) are in reasonably good agree-

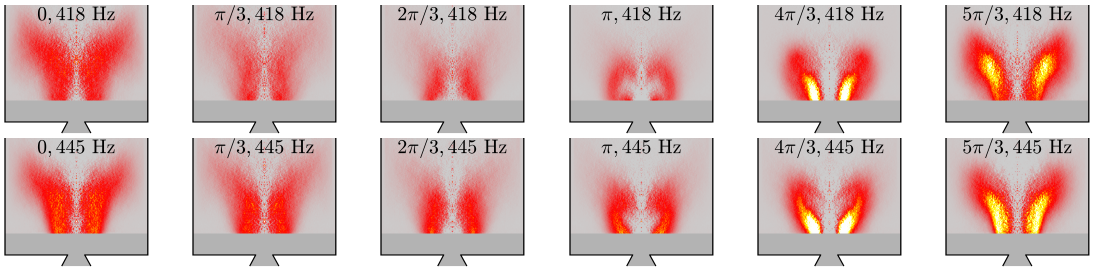

Figure 10: Phase averaged CH* chemiluminescence image of the flame in type (V) instability. The PiMax4 camera is triggered using the MP2 microphone signal. The averaging is conditioned by the frequency of the limit cycle oscillations, with the 418 Hz limit cycle at the top, and the 445 Hz limit cycle at the bottom. As the oscillation stays at each frequency for several seconds between switchings, well separated acquisition can be easily performed for each frequency. The images are obtained in the same manner as in Fig. 6. Swirler S_c at ($\mathcal{P} = 6.2\,\mathrm{kW}, \phi = 0.83, u_b = 42\,\mathrm{m\,s^{-1}}$).

Table 2: Acoustic simulation for swirler S_d: acoustic modes are determined experimentally by exciting the SICCA-Spray experiment with an external loudspeaker. Three operating conditions are considered: in the first column of the table, the plenum and the combustor are filled with air at room temperature, in the third column, the combustor is filled with a mixture of 24.4% air and 75.6% helium by volume such that the sound speed in this mixture is identical to that of the average temperature of the hot gases in the chamber (1000 K). Column 5 corresponds to acoustic simulations performed by considering that the combustor is filled with combustion products at a mean temperature of 1000 K. The experimental data resolution is $\Delta f = \pm 14$ Hz.

Air		Air & Helium		Hot fire
Exp.	Sim.	Exp.	Sim.	Sim.
250	248	260	246	240
284	273	434	464	461
		490	480	478
534	541	657	646	647
744	744	914	892	

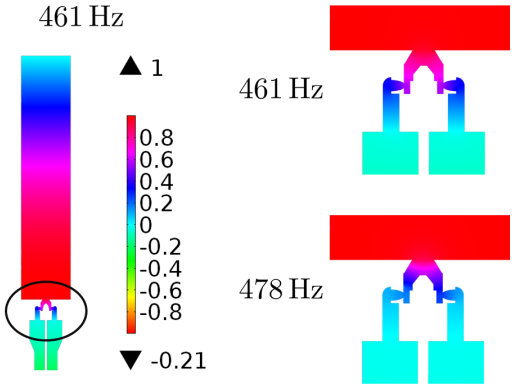

Figure 11: Acoustic pressure amplitude obtained in the simulations. The simulated domain is shown on the left for a frequency 461 Hz. On the right, the injector is shown in detail for the two eigenfrequencies of interest. The acoustic pressure is normalized by the acoustic pressure at the pressure antinode of each mode. Color version available online.

ment with simulation results (respectively columns 2 and 4). The frequency differences are less than 30 Hz in these two cases.

One may then calculate the eigenfrequencies under hot fire conditions by considering swirler S_d and assuming a mean temperature $T = 1000$ K in the chamber. This yields two eigenmodes at 461 Hz and at 478 Hz. These frequencies are not quite those observed experimentally but this could be expected since the instability frequencies are displaced with respect to the modal frequencies by the flame response. The two modes have nearly the same spatial structure. However the lowest eigenfrequency (461 Hz) corresponds to a mode that is coupled with the upstream plenum while the higher eigenfrequency (478 Hz) essentially pertains to a chamber mode (see the details Fig. 11). The higher amplitude of the acoustic pressure in the plenum is confirmed in Fig. 12 where the axial evolution of the acoustic pressure amplitude is shown.

This acoustic simulation indicates that two closely spaced acoustic modes coexist in the system. The lower frequency mode has a higher relative amplitude in the plenum. When the coupling between the plenum and the combustion chamber is strengthened, that is when the injector pressure loss is low, instabilities can more easily lock on this lower frequency mode, coupled with the plenum, leading to type (I) and type (IV) oscillations. In the experiment this pertains to the lower frequency oscillations at 418 Hz. When the injector pressure loss is higher, coupling between the cavities is diminished, leading to instabilities preferentially locking on the higher frequency, inducing type (II), and (III) combustion instabilities. These are manifested in the experiment at a frequency 445 Hz with in some cases a possible switching between the two eigenfrequencies (type (IV) oscillations).

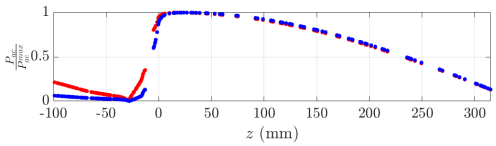

Figure 12: Axial evolution of the the acoustic pressure amplitude for the two modes. The acoustic pressure is normalized by its maximum in order to have the same scale for both curves. 461 Hz mode in red, 478 Hz mode in blue. $z = 0$ corresponds to the combustor backplane.

6. Conclusion

Effects of injector pressure losses are investigated in this article to see how changes in this parameter modify the combustion dynamics of a generic system. Four injectors are tested in a single element combustor fed with liquid fuel and air. The velocity profiles at the injector outlets are quite similar and the corresponding swirl numbers are nearly the same. Thus the steady flame shapes obtained with these four injectors are close to each other. However, their pressure losses vary by about 30%.

This setup allows to study the influence of the head loss as a design parameter while keeping the other conditions constant. The instability map of the burner is determined by examining the dynamical regimes and recording the various types of oscillations. The pressure loss in the injector has an impact on the occurrence, type and intensity of thermoacoustic instabilities. In this system, the range of global equivalence ratio corresponding to an unstable regime is wider for injectors with lower pressure loss. Four types of instabilities, coupled by two acoustic modes (418 Hz and 445 Hz) are observed. Calculations of the acoustic eigenmodes of the system indicate that two modes, that are close in frequency, coexist in this system. Both appear to have a quarter wave like structure. Oscillations at a frequency around 418 Hz, generally occurs when the injector pressure loss is low, and corresponds to a mode that weakly couples the chamber with the plenum. The second, at a frequency around 445 Hz, arises when the head loss is larger, and corresponds to a chamber mode. In a narrow domain, one also observes a random switching between the two modes. This bistable behavior might have been attributed to a change in flame response. However the flame shape is essentially identical in both types of instabilities and switching is linked to the existence of the two eigenmodes.

7. Acknowledgements

This work benefited from the support of SafranTech, and of project FASMIC ANR-16-CE22-0013 of the French National Research Agency (ANR).

[1] G. Sutton, O. Biblarz, Rocket propulsion elements, John Wiley and Sons, New-York, NY, USA, 1949.
[2] M. Summerfield, J Am Rocket Soc 21 (1951) 108–114.
[3] Harrje, D. T., Liquid propellant rocket combustion instability - NASA-SP-194, Technical Report, NASA, 1972.
[4] V. Yang, W. E. Anderson, Liquid Rocket Engine Combustion Instability, AIAA, Washington DC, USA, 1995.
[5] S. Candel, P. Combust. Inst. 29 (2002) 1–28.
[6] T. Poinsot, P. Combust. Inst. 36 (2017) 1–28.
[7] P. K. Tang, W. A. Sirignano, J. Sound Vib. 26 (1973) 247–262.
[8] V. Bellucci, C. O. Paschereit, P. Flohr, F. Magni, in: ASME Turbo Expo 2001, 2001-GT-0039, New Orleans, LA, USA.
[9] D. Zhao, A. S. Morgans, J. Sound Vib. 320 (2009) 744–757.
[10] N. Noiray, B. Schuermans, J. Sound Vib. 331 (2012) 2753–2763.
[11] D. Zhao, X. Y. Li, Prog. Aerosp. Sci. 74 (2015) 114–130.
[12] T. C. Lieuwen, V. Yang, Combustion Instabilities In Gas Turbine Engines, AIAA, Reston ,VA, USA, 2006.
[13] J. C. Oefelein, V. Yang, J. Propul. Power 9 (1993) 657–677.
[14] S. Tiribuzi, in: ASME Turbo Expo 2007, GT2007-280639, Montreal, Canada.
[15] N. Noiray, M. Bothien, B. Schuermans, Combust. Theor. Model. 15 (2011) 585–606.
[16] P. Wolf, G. Staffelbach, L. Y. M. Gicquel, J.-D. Müller, T. Poinsot, Combust. Flame 159 (2012) 3398–3413.
[17] D. Durox, J. P. Moeck, J. F. Bourgouin, P. Morenton, M. Viallon, T. Schuller, S. Candel, Combust. Flame 160 (2013) 1729–1742.
[18] W. Lang, T. Poinsot, S. Candel, Combust. Flame 70 (1987) 281–289.
[19] K. R. McManus, T. Poinsot, S. Candel, Prog. Energ. Combust. 19 (1993) 1–29.
[20] W. Polifke, A. Fischer, T. Sattelmayer, J. Eng. Gas Turb. Power 125 (2003) 21–27.
[21] T. Schuller, D. Durox, P. Palies, S. Candel, Combust. Flame 159 (2012) 1921–1931.
[22] T. Poinsot, D. Veynante, Theoretical and numerical combustion, R.T. Edwards, 2012.
[23] J.-F. Bourgouin, D. Durox, J. Moeck, T. Schuller, S. Candel, in: ASME Turbo Expo 2014, GT2014-25067, Düsseldorf, Germany.
[24] K. Prieur, D. Durox, T. Schuller, S. Candel, J. Eng. Gas Turb. Power 140 (2017) 031503.
[25] N. Noiray, D. Durox, T. Schuller, S. Candel, J. Fluid Mech. 615 (2008) 139.
[26] D. Laera, T. Schuller, K. Prieur, D. Durox, S. M. Camporeale, S. Candel, Combust. Flame 184 (2017) 136–152.
[27] K. Prieur, D. Durox, T. Schuller, in: Thermoacoustic instabilities in gas turbines and rocket engines: industry meets academia, Munich, Germany.
[28] S. Hermeth, G. Staffelbach, L. Y. Gicquel, V. Anisimov, C. Cirigliano, T. Poinsot, Combust. Flame 161 (2014) 184–196.
[29] A. Renaud, S. Ducruix, L. Zimmer, P. Combust. Inst. 36 (2017) 3899–3906.
[30] J. Y. Chung, D. A. Blaser, The Journal of the Acoustical Society of America 68 (1980) 907–913.